Contribution from the Dipartimento di Chimica Inorganica, Metallorganica ed Analitica, Università di Padova, Padova, Italy, Dipartimento di Chimica, Università della Basilicata, Potenza, Italy, Dipartimento di Scienze Chimiche, Università di Catania, Catania, Italy, Anorganisch Chemisch Laboratorium, University of Amsterdam, Amsterdam, The Netherlands, and Istituto di Chimica e Tecnologia dei Radioelementi del CNR, Padova, Italy

Experimental and Theoretical Investigation of the Electronic Structure of Two Isoelectronic Binuclear Clusters. UV-PES and DV-Xα Study of $Ru_2(CO)_6[\mu,\mu'$-N(R)CH_2CH_2N(R)] and $FeRu(CO)_6[\mu,\mu'$-N(R)CH_2CH_2N(R)]

M. Casarin,*[1a,b] A. Gulino,[1c] M. J. A. Kraakman,[1d] G. A. Rizzi,[1b] A. Vittadini,[1e] and K. Vrieze*[1d]

Received May 30, 1990

The electronic structure of two novel binuclear complexes, containing the diradical 6e-bonded μ,μ'-1,2-*ethanediyldiamido* [μ,μ'-N(*i*-Pr)CH_2CH_2N(*i*-Pr), hereafter R-EDA] ligand, is discussed by using SCF first-principle discrete variational (DV) Xα calculations and gas-phase UV-photoelectron (PE) spectroscopy. The nitrogen-metal interaction has been compared with that computed, within the same theoretical framework, for different isoelectronic complexes where the unsaturated 1,4-diaza-1,3-butadiene [N(*i*-Pr)=CHCH=N(*i*-Pr), hereafter R-DAB] ligand acts either as an 8e (σ-N, σ-N′, η^2-CN, η^2-CN′) or a 4e (σ-N, σ-N′ chelating) donor. Such a comparison indicates that different coordinative situations correspond to significantly different bonding schemes, pointing out that the versatile coordination behavior of the saturated (R-EDA)/unsaturated (R-DAB) ligand is a consequence of its "electronic flexibility". In particular, two interesting and unexpected points come out from the analysis of theoretical data. First of all, in both $Ru_2(CO)_6[\mu,\mu'$-N(R)CH_2CH_2N(R)] and $FeRu(CO)_6[\mu,\mu'$-N(R)CH_2CH_2N(R)] complexes, the main source of the M-N bonding is π in nature, while σ contributions are very poor. Second, in the former compound, a metal-based t_{2g}-like level actively participates in the Ru-N interaction. Transition-state ionization energies reproduce excellently the experimental PE pattern of the homobinuclear complex while some discrepancy is present between computed and experimental ionization energies in the heterobinuclear one.

Introduction

The electronic structure of metal carbonyl complexes with α-diimines ($RN_\alpha{=}C_\beta HC_\beta H{=}N_\alpha R$, hereafter R-DAB) has been investigated both theoretically and experimentally in a series of papers recently published.[2] The interest in these kinds of complexes is mainly due to the extremely versatile coordination behavior shown by the α-diimines, which can act as a 2e (σ-N),[3] 4e (σ-N, σ-N′ chelating),[3] 4e (η^2-CN, η^2-CN′),[4] 2e,2e (σ-N, σ-N′ bridging),[3] 6e (σ-N, μ_2-N′, η^2-CN′),[3] and 8e (σ-N, σ-N′, η^2-CN, η^2-CN′)[3] donors. Moreover, it has been shown that the coordinated α-diimine ligand may easily participate in not only C—H and N—H bond formation, but also in C—C and N—C coupling reactions with a wide variety of unsaturated organic substrates,[5,6] such as α-diimines,[7] carbodiimides (RN=C=NR),[8] sulfines ($R_2C{=}S{=}O$),[8] ketene ($H_2C{=}C{=}O$)[9] and alkynes (R′C≡CR″).[10]

Despite the large amount of work relative to the exploration of the chemical properties of the metal—η^2-C=N bonded unit, little is known about the hydrogen addition to the $N_\alpha C_\beta C_\beta N_\alpha$ skeleton of a coordinated R-DAB ligand. In relation to that, some of us showed quite recently that $FeRu(CO)_6$(R-DAB(6e)) reacts with H_2 (D_2) to give $FeRu(CO)_6(\mu,\mu'$-N(R)CHYCHYN(R)) (Y = H, D) involving selective trans addition of H_2 (D_2) across the central C-C bond of the $N_\alpha C_\beta C_\beta N_\alpha$ skeleton, while no loss of CO occurs.[11]

In this contribution, which is part of a systematic investigation of the electronic properties of metallacycle binuclear complexes,[2,12] we report a combined theoretical and experimental investigation of the electronic structure of the two novel binuclear complexes $Ru_2(CO)_6[\mu,\mu'$-N(*i*-Pr)CH_2CH_2N(*i*-Pr)] and $FeRu(CO)_6[\mu,\mu'$-N(*i*-Pr)CH_2CH_2N(*i*-Pr)] (hereafter I and II; see Figure 1), containing the diradical μ,μ'-6e-donor 1,2-*ethanediyldiamido* (hereafter R-EDA) ligand, by using SCF first-principle discrete variational (DV) Xα calculations and gas-phase UV-photoelectron (PE) spectroscopy. Incidentally, the strategy of coupling this theoretical method with UV-PE spectroscopy has been demonstrated in the past to be successful to obtain detailed information about the electronic properties of complex molecular systems.[13]

The main goal of the present contribution is the investigation of differences in the nitrogen-metal interactions on passing from the unsaturated R-DAB ligand acting either as a 8e (σ-N, σ-N′, η^2-CN, η^2-CN′) or a 4e (σ-N, σ-N′ chelating) donor to the "saturated" μ,μ'-6e-donor R-EDA. In this respect, we will make an extensive use of comparison with theoretical results, obtained within the same framework, relative to the electronic structure of a series of isoelectronic molecules: $Ru_2(CO)_4$(R-DAB)(μ-CO)[2a] (R = neopentyl, III), $Ru_2(CO)_4$(R-DAB)(μ-HC≡CH)[2a] (R = isopropyl, IV), and $Fe_2(CO)_4$(R-DAB)(C_4R_4)[2c] (R = isopropyl, V) (see Figure 1). Due to the low symmetry of the heterobinuclear complex II, which in principle allows extensive mixing of atomic orbitals (AOs), the character of selected molecular orbitals (MOs), particularly important to describe the metal-ligand (M-L) interactions, has been assigned by referring to the relative contour plots (CPs).

Experimental Section

UV-Photoelectron Spectra. High-resolution He I and He II excited PE spectra were measured by directly interfacing an IBM AT computer to a Perkin-Elmer PS-18 spectrometer modified for He II measurements by inclusion of a hollow-cathode discharge lamp, giving a high output of He II photons (Helectros Developments). Resolution measured on the

(1) (a) Università di Padova. (b) Università della Basilicata. (c) Università di Catania. (d) University of Amsterdam. (e) CNR.
(2) (a) Casarin, M.; Vittadini, A.; Vrieze, K.; Muller, F.; Granozzi, G.; Bertoncello, R. *J. Am. Chem. Soc.* **1988**, *110*, 1775. (b) Casarin, M.; Granozzi, G. *J. Chim. Phys.* **1989**, *86*, 841. (c) Bertoncello, R.; Casarin, M.; Dal Colle, M.; Granozzi, G.; Mattogno, G.; Muller, F.; Russo, U.; Vrieze, K. *Inorg. Chem.* **1989**, *28*, 4243.
(3) A review dealing with the chemistry of α-diimine ligands: Vrieze, K. *J. Organomet. Chem.* **1986**, *300*, 307 and references therein.
(4) Kokkes, M. W.; Stufkens, D. J.; Oskam, A. *J. Chem. Soc.* **1984**, 1005.
(5) Keijsper, J.; Grimberg, P.; van Koten, G.; Vrieze, K.; Christophersen, M.; Stam, C. H. *Inorg. Chim. Acta* **1985**, *102*, 29.
(6) (a) Keijsper, J.; Mul, J.; van Koten, G.; Vrieze, K.; Ubbels, H. C.; Stam, C. H. *Organometallics* **1984**, *3*, 1732. (b) Zoet, R.; van Wijnkoop, M.; Versloot, P.; van Koten, G.; Vrieze, K. *Organometallics*, in press.
(7) (a) van Koten, G.; Jastrzebski, J. T. B. H.; Vrieze, K. *J. Organomet. Chem.* **1983**, *250*, 49. (b) Staal, L. H.; Oskam, A.; Vrieze, K.; Roosendaal, E.; Schenk, H. *Inorg. Chem.* **1979**, *18*, 1634. (c) Staal, L. H.; Polm, L. H.; Balk, R. W.; van Koten, G.; Vrieze, K.; Brouwers, A. M. F. W. *Inorg. Chem.* **1980**, *19*, 3343. (d) Polm, L. H.; van Koten, G.; Elsevier, C. J.; Vrieze, K.; van Santen, B. F. K.; Stam, C. H. *J. Organomet. Chem.* **1986**, *304*, 353.
(8) Keijsper, J.; Polm, L. H.; van Koten, G.; Vrieze, K.; Schagen, J. D.; Stam, C. H. *Inorg. Chim. Acta* **1985**, *103*, 137.
(9) Polm, L. H.; van Koten, G.; Vrieze, K.; Stam, C. H.; van Tunen, W. C. J. *J. Chem. Soc., Chem. Commun.* **1983**, 1177.
(10) Staal, L. H.; van Koten, G.; Vrieze, K.; van Santen, B. F. K.; Stam, C. H. *Inorg. Chem.* **1981**, *20*, 3598.
(11) Zoet, R.; Elsevier, C. J.; van Koten, G.; Versloot, P.; Vrieze, K.; van Wijnkoop, M.; Duineveld, C. A.; Goubitz, K.; Heijdenrijk, D.; Stam, C. H. *Organometallics* **1989**, *8*, 23.
(12) (a) Casarin, M.; Ajò, D.; Vittadini, A.; Ellis, D. E.; Granozzi, G.; Bertoncello, R.; Osella, D. *Inorg. Chem.* **1987**, *26*, 2041. (b) Casarin, M.; Ajò, D.; Granozzi, G.; Tondello, E.; Aime, S. *Inorg. Chem.* **1985**, *24*, 1241.
(13) Granozzi, G.; Casarin, M. In *Topics in Physical Organometallic Chemistry*; Gielen, M., Ed.; Freund: London, 1989; pp 107-162 and references therein.

0020-1669/91/1330-1906$02.50/0

Table I. Atomic Character from the SCF DV-Xα Calculation of $Ru_2(CO)_6(\mu,\mu'\text{-}N(CH_3)CH_2CH_2N(CH_3))$

	eigenvalue		population, %							
			2Ru							
MO	$-E$, eV	TSIE	s	p	d	2N	$2(CH_2)$	$2(CH_3)$	6(CO)	character
$15b_1$[a]	2.90		1	6	17	9	0	1	66	
$19a_1$	6.37	8.75	3	18	40	0	0	0	39	Ru–Ru σ bond
$14b_1$	7.03	9.37	1	1	40	31	0	6	21	N_α pseudo-π → empty e_g-like
$10a_2$	7.05	9.38	0	2	16	48	10	11	13	N_α pseudo-π → empty e_g-like
$13b_2$	7.25	9.56	0	4	47	16	3	4	26	t_{2g}-like + N_α n^-
$18a_1$	7.25	9.54	1	7	41	21	3	4	23	t_{2g}-like + N_α n^+
$13b_1$	7.27	9.60	0	2	41	25	5	6	21	t_{2g}-like + N_α pseudo-π
$9a_2$	7.31	9.75	0	1	71	1	1	1	25	t_{2g}-like + CO $2\pi^*$
$12b_1$	7.57	10.02	0	0	75	0	0	1	24	t_{2g}-like + CO $2\pi^*$
$17a_1$	7.57	9.97	0	0	69	2	4	3	22	t_{2g}-like + CO $2\pi^*$
$12b_2$	9.72	11.96	0	1	28	30	3	16	22	N_α n^-
$16a_1$	10.35	12.60	1	1	20	28	29	8	13	N_α n^+

[a] Lowest unoccupied MO.

Table II. Atomic Character from the SCF DV-Xα Calculation of $RuFe(CO)_6(\mu,\mu'\text{-}N(CH_3)CH_2CH_2N(CH_3))$

	eigenvalue		population, %											
			Ru			Fe								
MO	$-E$, eV	TSIE	s	p	d	s	p	d	2N	$2(CH_2)$	$2(CH_3)$	$3(CO)_{Ru}$	$3(CO)_{Fe}$	character
34a″[a]	3.24		0	3	10	0	2	23	8	1	1	38	14	
33a′	6.58	9.03	0	4	11	0	1	55	3	1	0	13	12	$(t_{2g}\text{-like})_{Fe}$
23a″	6.66	9.21	0	0	4	0	0	68	6	1	1	2	18	$(t_{2g}\text{-like})_{Fe}$
32a′	6.67	9.29	0	0	2	0	1	70	3	2	1	0	21	$(t_{2g}\text{-like})_{Fe}$
31a′	6.93	9.44	1	4	8	1	15	40	3	0	1	10	17	Fe–Ru bond
22a″	7.43	9.74	0	4	12	0	2	7	37	8	9	17	4	N_α pseudo-π → Ru e_g-like
30a′	7.52	9.90	0	4	39	0	0	0	21	6	6	24	0	$(t_{2g}\text{-like})_{Ru}$ + N_α n^+
21a″	7.64	10.15	0	0	42	0	3	7	19	4	5	17	3	$(t_{2g}\text{-like})_{Ru}$ + N_α n^-
29a′	7.69	10.03	0	1	14	0	4	9	38	8	9	8	9	N_α pseudo-π → Fe e_g-like
28a′	7.94	10.69	0	0	68	0	0	0	1	2	2	26	1	$(t_{2g}\text{-like})_{Ru}$
20a″	10.04	12.29	0	0	12	0	1	5	36	4	20	17	5	N_α n^-
27a′	10.45	12.70	0	0	3	0	0	1	20	48	24	2	2	
26a′	10.90	13.20	0	0	6	0	2	3	33	7	25	14	10	N_α n^+

[a] Lowest unoccupied MO.

He $1s^{-1}$ line was always around 22 meV. The He II spectra were corrected only for the He II β "satellite" contributions (10% on reference N_2 spectrum). The ionization energy (IE) scale was calibrated by reference to peaks due to admitted inert gases (Xe–Ar) and to the He $1s^{-1}$ self-ionization. A heated inlet probe system was used at 90–110 °C.

Synthesis. Title compounds were synthesized according to the published procedures.[11] After crystallization, their purity was checked by IR and ^1H NMR spectroscopies.

Theoretical Method. SCF Hartree–Fock–Slater discrete variational (DV) Xα calculations[14] of I and II were performed on a VAX-8530 (Digital Equipments) computer at the computing center of the University of Basilicata.

The following approximations are used throughout the calculations: (i) the use of near-minimal AO basis sets, (ii) a self-consistent charge (SCC) approximation of the Coulomb potential, representing atoms by overlapping spherical charge distributions,[14b,15] (iii) the use of the Gaspar–Kohn–Sham exchange-correlation potential,[16] (iv) neglect of relativistic effects, and (v) Slater's transition-state (TS) formalism[17] to compute the ionization energies (IEs).

Numerical AOs (through 5p on Ru, 4p on Fe, 2p on C, N, and O, and 1s on H) obtained for the neutral atoms were used as basis functions. Due to the size of the investigated systems, orbitals 1s–4p (Ru), 1s–3p (Fe), and 1s for carbon, nitrogen and oxygen have been kept frozen in a fully occupied configuration, allowing their exclusion from the variational calculations. Valence states were constrained to remain orthogonal to the atomic cores. Atomic orbital populations were computed by using

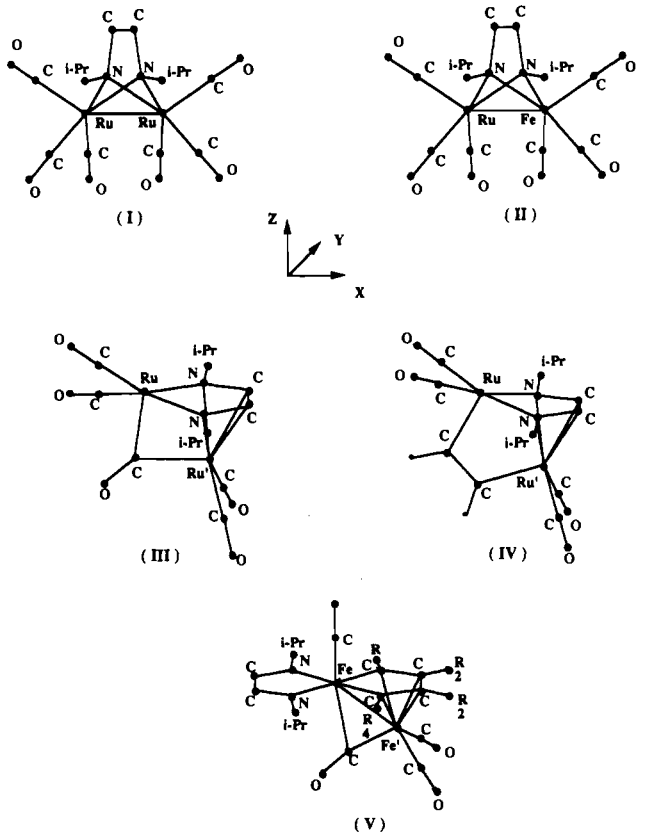

Figure 1. Schematic views of investigated molecules. The reference framework is also reported.

(14) Averill, F. W.; Ellis, D. E. *J. Chem. Phys.* **1973**, *59*, 6412. (b) Rosen, A.; Ellis, D. E.; Adachi, H.; Averill, F. W. *J. Chem. Phys.* **1976**, *65*, 3629 and references therein. (c) Trogler, W. C.; Ellis, D. E.; Berkowitz, J. *J. Am. Chem. Soc.* **1979**, *101*, 5896.
(15) Holland, G. F.; Manning, M. C.; Ellis, D. E.; Trogler, W. C. *J. Am. Chem. Soc.* **1983**, *105*, 2308.
(16) (a) Gaspar, R. *Acta Phys. Acad. Sci. Hung.* **1954**, *3*, 263. (b) Kohn, W.; Sham, L. J. *Phys. Rev.* **1965**, *140A*, 1133.
(17) Slater, J. C. *Quantum Theory of Molecules and Solids. The Self-Consistent Field For Molecules and Solids*; McGraw-Hill: New York, 1974; Vol. 4.

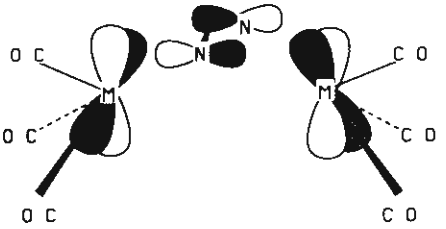

Figure 2. Qualitative drawing of the L → M donation of symmetry a_2 involving the pseudo-π N_α levels.

Mulliken's scheme,[18] and they are reported in Table I and II together with transition-state ionization energy (TSIE) values that have been computed for each occupied MO therein reported. Geometrical parameters for the title compounds were taken from ref 11 and idealized to the C_{2v} symmetry (I) and C_s symmetry (II), respectively. In order to save computer time, the electronic properties of the R substituents (R = isopropyl) on the nitrogen atoms have been simulated by replacing them with methyl groups. Such a procedure was already adopted during the theoretical investigations relative to III, IV, and V.[2]

Results and Discussion

A first, qualitative description of the bonding scheme of I and II can be obtained by using a well-trained method, i.e. the interacting fragment approach, which consists of dividing the whole molecules into interacting fragments and allowing the interaction of their outermost MOs. In the present case, the choice of the interacting fragments is straightforward: $RuM(CO)_6$ [M = Ru (I), Fe (II)] and R-EDA. The frontier MOs of the bimetallic fragment mainly involved with those of the bridging ligand have been thoroughly described by Hoffmann and co-workers.[19] According to their suggestions the $M(CO)_3$ subfragment "remembers its octahedral parentage" so that the metal-based orbitals can be labeled as e_g- and t_{2g}-like. The higher lying e_g-like set accounts for the M–CO σ-antibonding interaction, while the inner t_{2g}-like one consists of strongly metal-localized orbitals ("d pairs") mainly involved in the back-donation interaction into the virtual $2\pi^*$ CO-based levels. When two $M(CO)_3$ subfragments are allowed to interact to give rise to the $M_2(CO)_6$ unit, bonding and antibonding combinations (with respect to the M–M interaction) of the e_g- and t_{2g}-like sets are obtained. As far as those coming out from the t_{2g}-like set is concerned ($a_1 + a_1 + a_2 + b_1 + b_1 + b_2$; in our framework), their net contribution to the metal–metal bond in a d^8 system[20] is usually quite poor because both bonding and antibonding partners are completely occupied. The same thing does not hold for the e_g-like ones ($a_1 + b_2 + a_2 + b_1$; in our framework) where only the bonding combinations ($a_1 + b_2$) are as a result occupied.[21] Moreover, the e_g-like set is also significantly involved in the M–L interactions on passing from the $M_2(CO)_6$ unit to the actual complex $M_2(CO)_6$(ligand).[19]

In relation to R-EDA, six electrons are here available for coordination: four of them occupy the two $\perp$ lone pairs of the N_α atoms[22] (hereafter labeled as pseudo-π) of symmetry b_1 and a_2 in I and a′ and a″ in II, while the remaining two electrons fill up the in-phase linear combination of the $\parallel$ N_α "radical lobes" (hereafter n^+) of symmetry a_1. The out-of-phase linear combination n^- (b_2 in symmetry in our framework) is empty in the neutral diradical ligand. Elementary overlap and symmetry considerations allow us to expect the a_2 pseudo-π level to play a leading role in the M–N bond, giving rise to a highly delocalized interaction (see Figure 2).

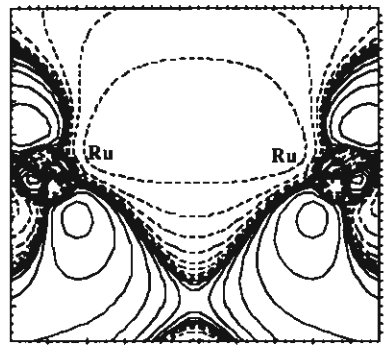

Figure 3. DV–Xα contour plot for the $19a_1$ MO in the *xz* plane. Contour values are $\pm3.2 \times 10^{-3}$, $\pm6.4 \times 10^{-3}$, $\pm1.28 \times 10^{-2}$, $\pm2.56 \times 10^{-2}$, $\pm5.12 \times 10^{-2}$, $\pm1.024 \times 10^{-1}$, $\pm2.048 \times 10^{-1}$, $\pm4.096 \times 10^{-1}$, and $\pm8.192 \times 10^{-1}$ $e^{1/2}/Å^{3/2}$ with negative values in dashed lines.

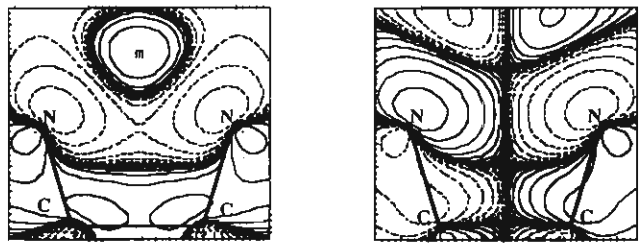

$18a_1$ $13b_2$

Figure 4. DV–Xα contour plot for the $13b_2$ and $18a_1$ MOs in the *yz* plane (m indicates the midpoint between Ru atoms). Plot parameters are identical with those of Figure 3.

As a whole we expect that, in both I and II, the 11 outermost MOs should be those coming from the $M_2(CO)_6$- plus the R-EDA-based levels (six t_{2g}-like + two e_g-like + two pseudo-π + n^+).

$Ru_2(CO)_6[\mu,\mu'$-N(R)CH_2CH_2N(R)]. In Table I the DV–Xα ground-state charge density analysis of the 12 highest lying MOs of I is reported. The theoretical results nicely match the aforesaid qualitative description. The highest occupied MO (HOMO, $19a_1$) is completely shared between the Ru atoms and the CO groups. This level is related to the e_g-like set, it is strongly concentrated between the Ru atoms, and it represents the direct Ru–Ru σ bond (see Figure 3). Moreover, accordingly to its e_g-like character, it is antibonding with respect to the Ru–CO σ interaction.

In relation to the analysis of the following eight MOs ($14b_1$–$17a_1$), it is useful to divide them into three different sets. The first one includes the $14b_1$ and $10a_2$ levels, which account for the donation from the N_α pseudo-π orbitals into the empty a_2 and b_1 e_g-like MOs of the bimetallic fragment. Accordingly, they represent, together with the $13b_1$ level (see below), the main source of bonding between the N_α and Ru atoms (their relative orbital overlap populations (OOP) are 0.184e and 0.092e, respectively). The second and the third set comprise the six t_{2g}-like orbitals. Among them the $9a_2$, $12b_1$, and $17a_1$ MOs (the third set) are purely t_{2g}-like in nature, almost completely localized on the Ru atoms (see Table I) and mostly involved in the back-bonding interaction into the $2\pi^*$ CO-based virtual levels. The analysis of the $13b_2$ and $18a_1$ MOs requires a special caution. They are the antibonding partners (see Figure 4) of the interaction between suitable levels belonging to the t_{2g}-like set and the n^+ and n^- linear combinations of the $\parallel$ N_α "radical lobes". Incidentally, the bonding counterparts, more localized on the organic fragment, are accounted for by the $12b_2$ and $16a_1$ MOs. The presence of bonding/antibonding partners involving n^- ($12b_2$ and $13b_2$ MOs, respectively) indicates that a better description of the bonding scheme is obtained by considering the R-EDA as formally charged 2– rather than neutral. Particularly interesting is the analysis of the nature of the last t_{2g}-like orbital, the $13b_1$ MO. This level accounts for a strong bonding interaction between the second b_1 level of the t_{2g}-like set of the bimetallic fragment (the other one gives rise to the $12b_1$ MO)[23] and the b_1 combination of the N_α

(18) Mulliken, R. S. *J. Chem. Phys.* **1955**, *23*, 1833.
(19) (a) Elian, M.; Hoffmann, R. *Inorg. Chem.* **1975**, *14*, 126. (b) Elian, M.; Chen, M. M. L.; Mingos, M. P.; Hoffmann, R. *Inorg. Chem.* **1976**, *15*, 1148. (c) Thorn, D. L.; Hoffmann, R. *Inorg. Chem.* **1978**, *17*, 126.
(20) Metal atoms are formally in their zero ion state both in I and in II.
(21) The e_g-like set of the $M(CO)_3$ subfragment (M = d^8) gives rise, in $M_2(CO)_6$, to two occupied MOs bonding in character with respect to the M–M interaction. If the $M_2(CO)_6$ has a C_{2v} symmetry, as in I, one of these MOs will be σ in character (symmetry a_1) while the other one will have a π nature (symmetry b_2 in our framework).[19c]
(22) $\perp$ and $\parallel$ symbols, perpendicular and parallel, respectively, refer to the R-EDA plane.

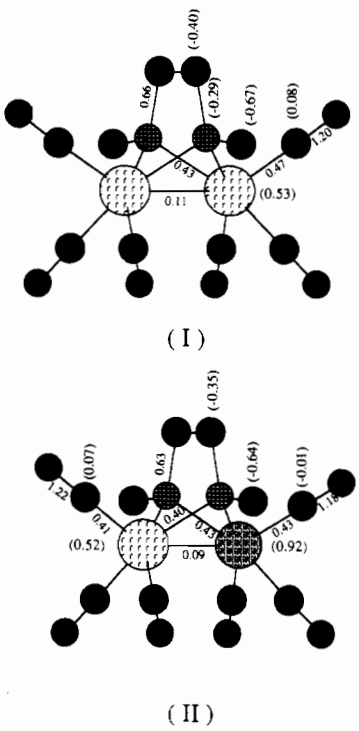

Figure 5. DV-Xα gross atomic charges (in parentheses) and total overlap populations of I and II.

pseudo-π orbitals. Such a fact is definitely unusual and deserves to be stressed because it implies that the t_{2g}-like orbitals, usually simple spectators of the M–L interactions, actively participate in the M–L bond. The antibonding partner of the interaction between the b_1 levels of the bimetallic fragment and the ligand-based b_1 pseudo-π orbital is the empty $18b_1$ MO, which shows, among the unoccupied MOs, the largest contributions from the Ru d_{xz} AOs (20%) as well as from the N_α $2p_x$ AOs (8%).

Before we move to the analysis of the experimental results, an important point coming out of the calculations has to be emphasized: the Ru–N bonding interaction is clearly between π orbitals of the ligand and d lobes of the metal atoms. As far as the σ character of the Ru–N bond is concerned, this is computed to be very poor. In this regard, by referring to Figure 5, where the Mulliken gross atomic charges and the total OP are reported, we observe that the total Ru–N OP is 0.43e and the sum of OOPs relative to $14b_1$, $13b_1$, and $10a_2$ is 0.41e. The comparison of the present theoretical results with those obtained within the same framework for III–V[2] is particularly interesting because it shows that different coordinative situations[24] correspond to significantly different bonding schemes, indicating that the versatile coordination behavior of the saturated (R-EDA)/unsaturated (R-DAB) ligand is the consequence of a sort of "electronic flexibility" of the $N_\alpha C_\beta C_\beta N_\alpha$ skeleton. Actually, in III and IV, we showed[2] that the interaction between N_α and the Ru atom within the metallacycle is mainly π in character. This was the consequence of the bad energy matching between Ru 4d AOs and N_α n^+ and n^- combinations; the latter being shifted toward lower energies by the strong $\pi_2 \rightarrow$ Ru′ donation (Ru′ is the second Ru atom). The absence of such a strong donation interaction in V allowed both σ and π contributions to play an important role in the M–L interaction.[2c]

The low IE region (up to 12 eV) of the He I/He II excited PE spectra of I is reported in Figure 6, where bands have been alphabetically labelled. Relative IE values are reported in Table III. With reference to other polynuclear carbonyl clusters,[13] it

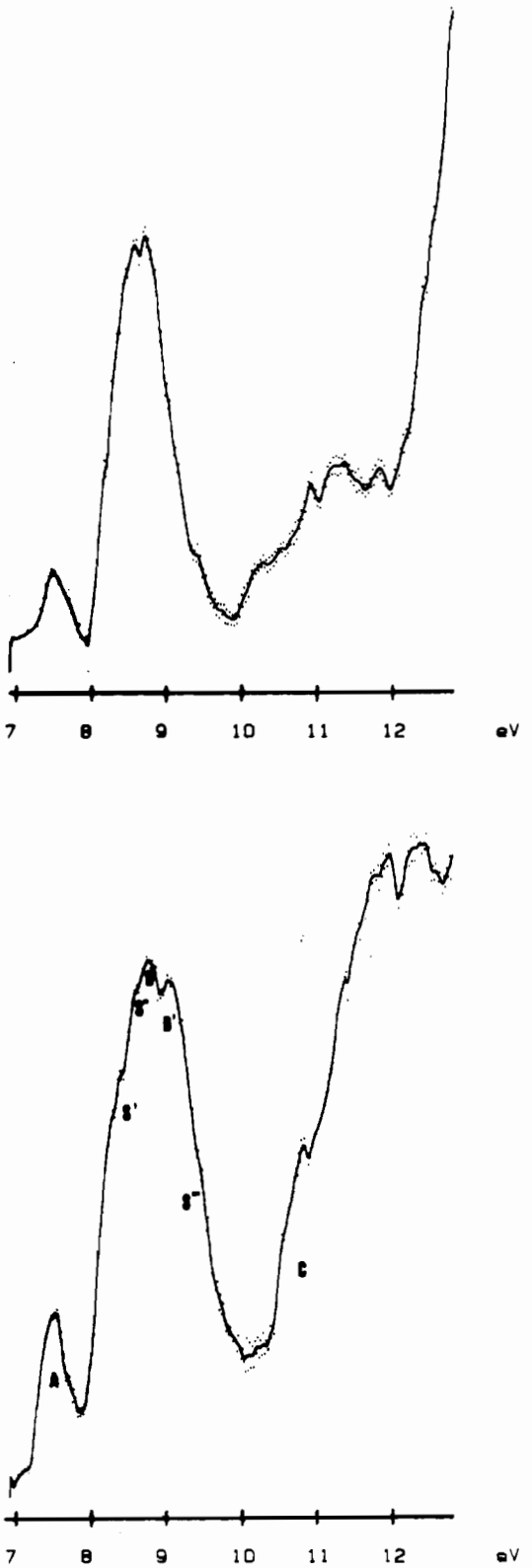

Figure 6. He I (below) and He II (above) PE spectra of I.

Table III. Ionization Energy Data (eV) for Compounds I and II[a]

band	I	band	II
A	7.52	A	7.5
(S′, S″) B	(8.39, 8.65) 8.77	B	8.1
B′ (S‴)	9.00 (9.5)		
C	10.79	(S, S′) C	(8.8, 9.0) 9.10
		D	10.8

[a] Shoulders in parentheses.

is well-known that the spectral region beyond 12 eV includes ionizations from levels primarily localized on the carbonyl groups

(23) The t_{2g}-like nature of the $12b_1$ and $13b_1$ MOs is confirmed by their bonding character with respect to the metal–carbonyl interaction.

(24) It is useful to remember that in III and IV the unsaturated R-(DAB) acts as an 8e (σ-N, σ-N′, η^2-CN, η^2-CN′) donor, while in V it works as a 4e (σ-N, σ-N′ chelating) donor.

(5σ, 4σ, and 1π MOs) as well as from the σ framework of the organic portion of the cluster. Since a detailed analysis of this region is not productive for the purposes of this contribution it has not been reported in Figure 6. The experimental pattern up to ≈10 eV is dominated by the presence of three well-defined peaks (A, B, and B′) centered at 7.52, 8.77, and 9.00 eV, respectively. Furthermore, at least three shoulders are evident, two on the lower IE side of band B (S′ and S″ in Figure 6) and one on the higher IE side of band B′ (S‴). TSIE calculations[17] (see Table I) reproduce very well this trend in relation to relative intensities and position of bands. Absolute IE values are, however, uniformly overestimated here by ≈1 eV.

On the basis of the above reported discussion and with reference to the PE results of similar $M_2(CO)_6L$ derivatives,[2a-c,13,25] no doubt at all exists in relating the low-intensity peak A to the ionization from the $19a_1$ MO, which, as already mentioned, accounts for the direct Ru–Ru σ bond. Bands B′ and B″ together with their shoulders are assigned as a whole to the ionization from the three sets previously described ($14b_1$–$17a_1$ MOs). In particular, band B′ and the shoulder S‴ are associated with the third set ($9a_2$, $12b_1$, and $17a_1$ MOs). These levels are highly localized on the Ru atoms (purely t_{2g}-like in character; see above), and accordingly, band B′ shows a relative intensity increase with respect to band B under the He II ionizing source.[26]

The marked decrease in relative intensity of the shoulder S′ indicates that it includes ionizations from MOs with significant contributions from ligand based levels.[26] On this basis and with reference made to the TSIE ordering, we propose to assign S′ to the ionization from the $14b_1$ and $10a_2$ MOs. Finally, the peak B and its shoulder S″ are assigned as a whole to the $13b_2$, $18a_1$, and $13b_1$ MOs which consistently are computed to be very close in energy.

Relying on TSIE ordering, we can reasonably assume that the bonding combination of the Ru–N_α σ interaction ($12b_2$ and $16a_1$ MOs; see Table I) are hidden under the broad and unresolved band envelope C beyond 10 eV, which in agreement shows a dramatic decrease in relative intensity on switching to the He II radiation.[26]

$RuFe(CO)_6[\mu,\mu'$-N(R)CH_2CH_2N(R)]. The analysis of the electronic structure of II can be easily worked out by making reference to the bonding scheme already proposed for I and keeping in mind well-known differences between Fe and Ru atoms. In Table II, the DV–Xα ground-state charge density analysis of the 13 high lying MOs of II is reported. We needed to add a further level (26a′ MO) in Table II in order to include MOs having the same character of those reported in Table I.

The outstanding difference between Table I and Table II is quite obvious: there is here a net energy separation between Fe-based t_{2g}-like levels (the higher lying 33a′, 23a″, and 32a′ MOs)[28] and the Ru-based ones (the lower lying 30a′, 21a″, and 28a′ MOs).[28] Moreover, the 31a′ MO, which is the main source of bonding between Fe and Ru (the relative OOP is 0.21e),[29] is asymmetrically distributed between the metal atoms. Such an asymmetry will give rise to a remarkable polarization of the metal–metal bond, which explains, at least partially, the significant difference in metal gross atomic charges (see Figure 5). Now, if we qualitatively assume that the direct Ru–Fe interaction arises from a charge

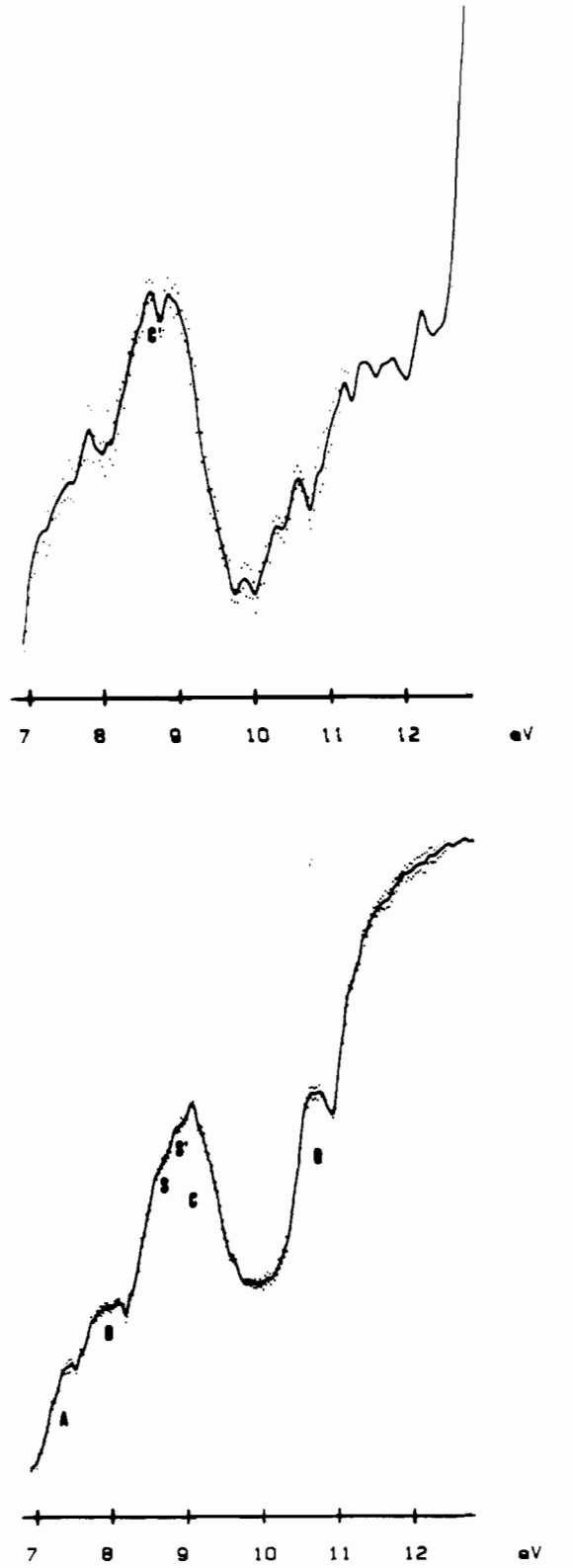

Figure 7. He I (below) and He II (above) PE spectra of II.

sharing between the e_g-like lobes of the $M(CO)_3$ subfragments,[19c] the obtained results are in concert with the higher electronegativity of Ru compared to that of Fe (Pauling values: Ru, 2.2; Fe, 1.8).[30] As already found in I, both N_α pseudo-π orbitals are involved in the ligand → metal donation, giving rise, in the present case, to two different bonding combinations, one that favors the charge transfer into an e_g-like level of Ru (the 22a″ MO, the relative M-N

(25) Casarin, M.; Ajò, D.; Vittadini, A.; Granozzi, G.; Bertoncello, R.; Osella, D. *Inorg. Chem.* **1986**, *25*, 511. Granozzi, G.; Casarin, M.; Aime, S.; Osella, D. *Inorg. Chem.* **1982**, *21*, 4073.

(26) In fact, on the basis of the Gelius mode,[27a] we expect a marked decrease in the cross-section ratio $\sigma(N\ 2p)/\sigma(M\ nd)$ on passing from the He I to the He II excitation source.[27b]

(27) (a) Gelius, U. In *Electron Spectroscopy*; Shirley, D. A., Ed.; North Holland: Amsterdam, 1972; p 311. (b) Rabalais, J. W. In *Principles of UV Photoelectron Spectroscopy*; Wiley Interscience: New York, 1977.

(28) The t_{2g}-like character of these MOs has been assigned on the basis of their localization percentage on the metal atoms as well as on the carbonyl groups.

(29) The total Fe–Ru OP is 0.09 (see Figure 5 for II). The smaller value with respect to the OOP relative to the 31a′ MO is due to the presence, among the occupied levels, of MOs antibonding in nature with respect to the Fe–Ru interaction.

(30) Johnson, B. F. G.; Lewis, J. *Adv. Inorg. Chem. Radiochem.* **1981**, *24*, 225.

OOPs are 0.11e (Ru), 0.05e (Fe)) and the other one, which mainly involves an e_g-like level of Fe (the 29a′ MO accounts for the largest Fe–N OOP among the occupied MOs (0.16e)). The strong interaction between a Fe-based e_g-like level and the symmetric combination of N_α pseudo-π orbitals can be explained by once more making reference to the larger charge of Fe compared to that of Ru. Moreover, the Fe–Ru bond polarization could be responsible for the slightly weaker Ru–N interaction,[31] which as a whole passes from 0.43e to 0.40e.[32]

Such a fact would also explain minor variations in the N–C(H)$_2$ OPs on passing from I to II (see Figure 5). In this regard, it is useful to remind that the N_α pseudo-π levels are the antibonding partners of the "π" interaction between N_α and $C_\beta(H)_2$; as a consequence the final N_α–$C_\beta(H)_2$ OP and the N_α and $C_\beta(H)_2$ gross atomic charges are the results of a subtle balance of bonding/antibonding interactions between the metals and N_α atoms.

As a final remark, even though the main source of bonding between metals and the R-EDA ligand is once more basically π in character, it is worthwhile to mention that in the present case no t_{2g}-like orbital seems to be involved in the M–L interaction. As already found in many other cases,[2,12] this result confirms that the M–L interactions are significantly influenced by the nature of the metal–metal bond.

Moving on to the discussion of PE experimental results of II (Figure 7, Table III), we see that the proposed bonding scheme nicely matches PE spectral pattern variations on going from I to II. Moreover, the considerations above reported in relation both to the energy region beyond 12 eV and to the uniform overestimate of the experimental IEs hold once more.

At a first look, the low-IE region of the He I/He II spectrum of II seems to be less resolved than in I. On the other hand, this is simply the consequence of the theoretically predicted (see above) different relaxations undergone by the 3d AOs with respect to the 4d ones. As a final issue, the ionizations from Fe-based MOs lie in the lower IE region of the spectrum, hiding the ionization from the MO responsible for the direct Fe–Ru σ bond (31a′ MO in Table II). As a whole, three bands (A, B, and C) are detectable in the IE region below 10 eV; a fourth well-defined band (D) lies at 10.8 eV. Moreover, at least two evident shoulders (S and S′ in Figure 7) are evident on the lower IE side of band C. There is no doubt in relating band A plus band B to the ionizations from the Fe t_{2g}-like orbitals (33a′, 23a″, and 32a′ MOs) as well as to the 31a′ MO. More specifically, band A could be associated with a single ionization event (33a′ MO), while band B could be associated with the ionization from the remaining three MOs. The increase in relative intensity of both bands with respect to the remaining ones on passing to the He II radiation is in tune with such an assignment.[33] On passing to the band envelope C, we propose to assign it as a whole to five ionization events (22a″–28a′ MOs) on the basis of its higher intensity with respect to bands A and B. As to a more detailed assignment of this band, it seems that the TSIE ordering does not completely agree with the relative intensity variations on passing from He I to the more energetic radiation. In fact, it is well evident that there is a significant increase in relative intensity of the lower IE region of band C so that, rather than two shoulders, an evident new peak (C′) is present in the He II spectrum. On this basis, we would be inclined to assign C′ to the ionzation of at least two Ru t_{2g}-like levels[26] and C to the remaining three orbitals, two of them being the pseudo-π levels of the N_α atoms. As far as this discrepancy is concerned, we would like to point out that (i) the computed energy difference between the 22a″ MO (significantly localized on the Nα 2p AOs) and the t_{2g}-like levels nearest in energy (30a′ and 21a″ MOs) is on the order of 0.2/0.3 eV and (ii) the ΔE between peaks C′ and C is almost the same (see Table III). An inversion in the TSIE ordering for levels so close in energy is not dramatic, and it can be due to the use of the SCC approximation to model the true electron density.

Finally, band D, on the basis of its dramatic decrease under the He II radiation and its energy position as well, is assigned with confidence to ligand-based orbitals. Making reference to TSIE results, we tentatively propose to assign the low-energy side of this band to the ionization from the 20a″ MO, which represents the out-of-phase linear combination of N_α lobes.

Conclusions

Theoretical data indicate that, in both I and II, the main source of bonding between the N_α atoms of the R-EDA ligand and the metals of the $M_2(CO)_6$ fragment is π in character. Moreover, as far as I is concerned, calculations point out that one of the metal-based t_{2g}-like orbitals is highly involved in the just mentioned bonding interaction. The overall bonding scheme, on going from I to II, is substantially the same, and slight differences can be rationalized by making reference to the presence of a polarized Ru–Fe bond. As a whole, DV–Xα results confirm once more that in polynuclear organometallic clusters the strength of the metal–metal interaction can influence the nature of the M–L bond. The comparison between experimental results and theoretical outcomes is excellent for I and acceptable for II. Such a difference does not have to be ascribed to the failure of the DV–Xα calculations in describing the mixing between ligand- and metal-based orbitals for low-symmetry molecules. Actually, in the recent past, we showed[2,12] that the DV–Xα method is "head and shoulders" above other computational techniques for obtaining quantitative informations about the bonding schemes of very complex molecular systems. In our opinion, the discrepancy between TSIE ordering and the relative intensity variations on passing from the He I to the He II ionizing source is a consequence of the approximations used throughout the calculations.

Acknowledgment. Thanks are due to Mr. G. Miglionico of the Computing Centre of the University of Basilicata for its invaluable technical assistance.

Registry No. I, 132438-44-9; II, 117341-42-1.

(31) The largest contribution to the Ru–N interaction in I and II comes from the $10a_2$ and 22a″ MOs, whose OOPs are 0.18e and 0.11e, respectively.
(32) It is worthwhile to mention that the Ru–N_α bond distances are almost exactly the same on going from I to II.
(33) It is well-known that Ru has a higher covalency than Fe, so that the stronger mixing between Ru and L AOs gives rise to MOs with a significant participation of ligand-based AOs.